Global Journal of Researches in Engineering: C
Chemical Engineering
Volume 23 Issue 1 Version 1.0 Year 2023
Type: Double Blind Peer Reviewed International Research Journal
Publisher: Global Journals
Online ISSN: 2249-4596 & Print ISSN: 0975-5861

Evaluation of the Corrosion Behavior on Austenitic Stainless Steels in Artificial Oil Field Formation Water using Potentiodynamic and Potentiostatic Electrochemical Techniques

By Jorge Luiz Cardoso, Luís Flávio Gaspar Herculano, Pedro de Lima Neto & Marcelo José Gomes da Silva

Federal University of Ceará

Abstract- *Objective:* The main objective of this research was to evaluate the corrosion resistance of some austenitic and super austenitic stainless steel when immersed in an aqueous solution of artificial oil field formation water saturated with CO_2 and also without CO_2. With these two simulated situations, the pH effect of the solution on the corrosion resistance of the alloys was studied.

Methods: Samples of austenitic and super austenitic stainless steels previously characterized by x-ray diffraction using synchrotron light were used in this research. Two electrochemical techniques, one potentiodynamic and the other potentiostatic were used to investigate the effect of the solution on the corrosion behavior of the samples.

Keywords: *austenitic stainless steels, CO_2 corrosion resistance, aqueous solution, pitting corrosion, potential step, passive layer.*

GJRE-C Classification: *NLM: WC 800*

Strictly as per the compliance and regulations of:

Evaluation of the Corrosion Behavior on Austenitic Stainless Steels in Artificial Oil Field Formation Water using Potentiodynamic and Potentiostatic Electrochemical Techniques

Jorge Luiz Cardoso [α], Luís Flávio Gaspar Herculano [σ], Pedro de Lima Neto [ρ] & Marcelo José Gomes da Silva [ω]

Abstract- ***Objective:*** The main objective of this research was to evaluate the corrosion resistance of some austenitic and super austenitic stainless steel when immersed in an aqueous solution of artificial oil field formation water saturated with CO_2 and also without CO_2. With these two simulated situations, the pH effect of the solution on the corrosion resistance of the alloys was studied.

Methods: Samples of austenitic and super austenitic stainless steels previously characterized by x-ray diffraction using synchrotron light were used in this research. Two electrochemical techniques, one potentiodynamic and the other potentiostatic were used to investigate the effect of the solution on the corrosion behavior of the samples. The linear polarization test was used to evaluate the CO_2 corrosion resistance of the alloys in artificial oil field formation water. The potentiostatic technique (potential step) was used to assess the influence of the solution without CO_2 on the corrosion resistance of the alloys, thus, varying the pH of the electrolyte. Scanning Electron Microscopy (SEM) was used to observe the type of corrosion on the surface of the samples.

Results: The results indicated that the type of corrosion found on the surface of the alloys was pitting corrosion. The pH effect of the solution (artificial oil field formation water) influenced the pits' shape. The conventional austenitic steels showed to have low corrosion resistance in chloride-containing environment. The super austenitic stainless steels presented a high corrosion resistance in the solution with and without CO_2. No pits or micro pits were observed on their surfaces by SEM.

Conclusion: From the results obtained, it was evident that the conventional austenitic stainless steels are not a good choice in severe environments like those found in the pre-salt region. The super austenitic stainless steels showed to be a good option in CO2-containing environments, mainly in aqueous solution with a high content of chloride.

Keywords: austenitic stainless steels, CO_2 corrosion resistance, aqueous solution, pitting corrosion, potential step, passive layer.

Author α σ ω: Department of Metallurgical and Materials Engineering, Federal University of Ceará, Fortaleza, CE, Brazil.
e-mail: jorgeluizjlc@gmail.com
Author ρ: Department of Analytical Chemistry and Physical Chemistry, Federal University of Ceará, Fortaleza, CE, Brazil.

I. Introduction

The discoveries made in the pre-salt region (a geological formation of continental shelves) in Brazil are among the world's most important in the past decade. In this region, there is a considerable amount of good quality oil and this reality puts Brazil in a strategic position for the global demand for energy [1]. The discovery of this region brings several technological challenges for the oil and gas exploration. The corrosion process in this region occurs under specific conditions. Some of them are high temperatures between 80°C and 150°C, the presence of gases such as carbon dioxide (CO_2) and hydrogen sulfide (H_2S), oil formation water, high pressure, leaving the operating environment very hostile[2]. The main characteristic of the pre-salt region is the high content of sodium chloride (NaCl) found there. This NaCl, CO_2 and H_2S dissolved in the oil field formation water can accelerate the corrosion of metallic materials used for the oil exploration in the pre-salt region. Another concern for this operation is the environmental impact that can occur if these materials fail. Cheaper materials such as carbon steels are a good choice but there is a problem related to them: The difficulty in adding corrosion inhibitors for carbon steel pipes in offshore oil extraction at great depths. This has led to the increased use of corrosion resistant alloys[3]. Of all types of corrosion, localized corrosion, especially pitting corrosion, is the most common in marine waters and difficult to control. Currently, the oil and gas industry is concerned about the environmental impact caused by oil leaks in the marine ecosystem. This type of accident can be prevented using materials more resistant to the environmental conditions found in the pre-salt region. There are two types of technological challenges for the exploration of oil and gas contained in the pre-salt region: the other challenge consists of drilling the well as far as the reservoir, crossing water layers, sediment, and salt. Each layer with a different behavior at temperatures ranges from 50°C to 150°C under high pressures and corrosive gases, all these conditions acting together. The way back to the surface must also be considered.

All the oil and natural gas extracted from the well will be transported through the pipelines, and the material from which the pipes are made must resist all adverse conditions to avoid oil leaks. The second challenge is horizontal and consists of transporting the oil and gas from the production area to the coast, localized about 300 km away from the well location [1]. In summary, it is a set of problems that begins with the well's depth, passing by the coating when drilling into soft sediments through the salt layer to reach a very high temperature and pressure environment saturated with corrosive gases already mentioned[4]. Corrosion resistant-alloys such as super austenitic stainless steels are a great choice when considering the severe conditions of pre-salt. Due to their high chromium, nickel, and molybdenum content, it is expected that this kind of material presents more corrosion resistance in the pre-salt conditions than the conventional stainless steels. Some authors have already studied the corrosion resistance of austenitic stainless steel and other materials regarding the effect of CO_2[1,5–8]. For this paper, the effect of the oil field formation water with and without CO_2 was studied, taking into account two austenitic and two super austenitic stainless steels for later comparison. Two electrochemical techniques, one potentiodynamic and the other potentiostat were used to evaluate the corrosion resistance for these materials in artificial oil formation water.

a) Materials

For this research, the materials used were the AL-6XN PLUS™ super austenitic stainless steel, the 904L super austenitic stainless steel, and the 300 series austenitic stainless steels AISI 316L and 317L. The chemical composition of the materials studied presented in Table 1 were measured in an Optical Emission Spectrometer (PDA-7000 SHIMADZU). The Pitting Resistance Equivalent Number (PRE_N) was calculated using equation 1.

$$PREN = \%Cr + 3.3\,Mo + 30\%N \quad \text{(Eq.1)}$$

Table 1: Chemical composition (wt%) of the studied alloys and the respective Pitting Resistance Equivalent Number (PRE_N)

Alloys	C	N	Mn	Si	Cr	Ni	Mo	PRE_N
316L	0.030	0.05	1.65	0.41	17.2	10.7	2.2	26
317L	0.024	0.06	1.49	0.40	17.8	12.3	3.5	31
904L	0.027	0.10	0.74	0.66	19.5	24.3	4.5	37
AL-6XN PLUS™	0.021	0.24	0.35	0.32	21.8	25.8	7.6	54

b) Characterization of the Samples

The samples in the as-received condition were characterized using x-ray diffraction (XRD) by Synchrotron Light (energy 12 keV) to detect the phases. ICDD database (International Centre for Diffraction Data) was used to identify the peaks of the phases. A Gleeble was used to fix the samples. The measurements were carried out at the Brazilian Synchrotron Light Laboratory in the city of Campinas-SP in Brazil. For this characterization, the shape and dimensions of the samples are shown in Figure 1.

c) Electrochemical Tests used

To evaluate the corrosion behavior of the materials, two electrochemical techniques were used: a potentiodynamic technique (linear polarization test) and a potentiostatic technique (potential steptest), one complementing the other. Firstly, the linear polarization technique was used to evaluate the effect of CO_2 on the corrosion behavior of the samples. The dimensions of the samples were 5.0 mm x 5.0 mm x 3.5 mm with an average exposure area of 39 mm^2. The samples were mounted in cold resin and ground using SiC paper up to 600 mesh, washed in distilled water, and then blow-dried. An adapted cell was used with two gas inlets, one for CO_2 and one for N_2. The cell also contained an input for a pH reader, in addition to the classic inputs for the three main electrodes (reference, working, and counter electrodes) in addition to a gas outlet (see Figure 2).The electrodes used were the samples (working electrode), as counter electrode a platinum electrode (93 mm^2), and the reference electrode used was the silver chloride silver (Ag/AgCl/Cl^-sat) saturated with KCl. The electrolyte used (artificial oil field formation water) was named by Petrobras of TQ 3219 which composition is shown in Table 2.

Table 2: Chemical composition of the artificial oil field formation water for 1 L of distilled water

Reagents	$CaSO_4$	$MgCl_2$	$NaHCO_3$	NaCl
C (g/L)	0.516	4.566	0.425	29

First, the solution was deaerated with N_2 gas to simulate the pre-salt environment (absence of free O_2) that could interfere with the results. The N_2 gas was bubbled into the solution until a pH of 8.2 ± 0.1. After this procedure, the solution was bubbled with CO_2 until saturation (pH 5.1 ± 0.1). In this procedure, the electrolyte became acidic. CO_2 gas in contact with an aqueous solution (oil field formation water) forms acids

that react with the metallic elements of the alloy [9]. A potentiostat (AUTOLAB PGSTAT302N) connected to a microcomputer was used for both techniques. The software NOVA 1.9 was used to obtain data from the linear potential curves. Before the measurements, the samples were immersed for 30 min in the solution to determine the open circuit potential (OCP). The sweep of the polarization curves was -0.5 V to 1.2 V from the OCP with a sweep rate of 1 mV/s. After linear polarization tests, the samples were washed with water and sprayed with alcohol to clean the surface. Scanning Electron Microscopy (SEM) micrographs on the surfaces of the samples were obtained after corrosion tests for later comparison. The corrosion tests were reproduced in triplicate.

The potential step technique (potentiostatic technique) was also used to evaluate the corrosion behavior of the samples for the solution of artificial oil field formation water, this time with no CO_2 and no N_2. This test was intended to evaluate only the effect of the artificial oil field formation water on the surface of the samples. For this test, the samples were mounted in cold-curing epoxy resin, ground up to 600, rinsed with ethanol, and blow-dried before each measurement. The samples had the dimensions of 8.3 mm x 8.2 mm x 3.7 mm. To reduce crevice corrosion on the epoxy/steel, the specimens were coated with a lacquer leaving an exposed area of 1 cm^2. A three-electrode cell configuration was used. A saturated silver/silver chloride (Ag/AgCl) as reference electrode and a platinum electrode as a counter electrode were used. The electrolyte used was the same used in the linear polarization test (see Table 2). A potentiostat (AUTOLAB PGSTAT302N) connected to a microcomputer along with the software NOVA 1.9 was used. Before the measurements, the samples were immersed for 30 min in the solution to determine the open circuit potential (OCP), the same procedure used before. Subsequently, the potential was increased in steps of 50 mV every one hour until a breakthrough current density was attained. The pitting corrosion initiation potential was defined when the current density reached values above 0.1 mA/cm^2 [10]. After the tests, the samples were examined by SEM to confirm the presence of pits on their surfaces. The tests were carried out in triplicate at 25°C (room temperature).

II. Results and Discussion

a) Characterization of the Samples for the as-received Conditions

The X-ray diffractogram pattern for the 316L and AL-6XNPLUS™ steels can be seen in Figure 3. For both sheets of steels, the main phases detected were the matrix phase (austenite) and some ferrite peaks, indicating that both materials were not in the solution annealed condition. No other phases were detected for the analyzed angle range 2Θ (25-79°). For this measurement, a synchrotron light radiation source (λ = 0.10332 nm) was used. This measurement was not possible for the 317L and 904L steels due to a manufacturing problem of the samples.

b) pH Study of the Solution

Firstly, the solution pH used in the corrosion tests (artificial oil field formation water) was studied. The solution was deaerated by bubbling N_2 to simulate the absence of free oxygen from the pre-salt layer. Figure 4 shows the results for the pH study of the solution (called TQ3219 by Petrobras). The stabilization of pH indicates that the electrolyte is deaerated and subsequently saturated with CO_2. All the chemical reaction that happens when bubbling CO2 in the solution is described in our previous work [4].

c) CO_2 Corrosion Evaluation using a Potentiodynamic Technique

Before the linear polarization tests, the OCP of the samples was measured. The result is shown in Figure 05. The OCP of the super austenitic steels (AL-6XN PLUS™ and 904L) stabilize in 5 minutes. For the other austenitic steels (316L and 317L), the stabilization time is longer, eespecially for the 317L steel. After 30 minutes of immersion, all the OCP are stabilized. Figure 6 shows the linear polarization curves for the steels in the as-received condition. The linear polarization tests aim to verify the formation of passive film or not on the alloys surfaces[11]. For this test, all the samples were immersed in the solution used (artificial oil field formation water) saturated with CO_2. The super austenitic stainless steels AL 6XN PLUS™ and 904L showed a good CO_2 corrosion resistance. After reaching the corrosion potential (around -0.5 V), a passive film is formed and broken at -0.34 V until they reach a passivation peak around -0.20 V. After this potential, there is the formation of another passive layer that remains until the potential of +0.89 V where there is a slight breakdown of this layer and another passivation. After reaching a potential of +1.02V (pitting potential), there is an increase in current density, the transmissive region, since the potential is too high (above +1.0 V). It is possible to observe that the electrochemical behavior for the super austenitic steels studied in this work is very similar. Their passive regions are quite stable. The increase of current density after +1,0 V can be associated with oxygen evolution, reported in the literature[12]. The 317L steel also showed a good CO_2 corrosion resistance. The formation of its passive layer is not so stable as the passive layers of the super austenitic steels; even so, the current density in the passive region remains low, in the order of 10^{-6} A/cm^2. Its pitting potential is around +0.61 V. The 316L steel did not present any passivation since the anodic current increased with time. This steel presented the highest anodic current rate (in the order of 10^{-5} A/cm^2) if

compared with the other steels. Its corrosion potential is similar to the corrosion potential of 317L steel (+0.40 V). 316L steel presented the lowest pitting potential (+0.30 V), indicating that its CO_2 corrosion resistance is not very efficient. The reduction in anodic current density is associated with the passive film as a protective barrier against corrosion. The super austenitic steels AL-6XN PLUS™ and 904L showed a reduction in their anodic current, while the austenitic steels 316L and 317L showed an increase in anodic current with time. This result shows that the passive film of super austenitic steels is more stable. This effect can be attributed to the high levels of alloying elements such as Cr, Mo, and Ni. According to Sedriks, on a polarization curve, the greater the difference between the pitting potential and the corrosion potential ($\Delta E = E_{pit} - E_{corr}$), the more resistant to corrosion the material is [13]. Table 2 shows the corrosion potential values, pitting potential, and the difference between them for the studied steels. The ΔE interval is higher for the super austenitic steels, which confirms their high performance about CO_2 corrosion. The 316L steel had the lowest value for ΔE, indicating that it is not a suitable material for applications that require good CO2 corrosion resistance. More detailed work on CO_2 corrosion using austenitic stainless steels by the authors of this research can be found in [4].

Table 2: Potentials in V (Ag/AgCl) taken from the linear polarization curves for the studied steels

Alloy	E(corr)	E(pit)	ΔE
316L	-0.41	0.30	0.71
317L	-0.41	0.61	1.02
904L	-0.49	1.02	1.51
AL-6XN PLUSTM	-0.53	0.99	1.52

After the linear polarization tests, SEM of the surfaces of the steels was carried out. The only material that presented pits on its surface was the 316L steel, as shown in Figure 7. Several factors may have influenced this form of corrosion for the 316L steel. Among them, one can mention: inefficiency of the passive film, pH of the solution, chloride content in the solution, effect of CO_2. The action of the chloride ion in an acid medium caused by the reaction of CO_2 gas in an aqueous medium can accelerate the localized corrosion process.

d) The Corrosion Resistance of the Steels in Artificial Oil Field Formation Water by Potential Step Technique

The samples in the as-received condition were submitted to another electrochemical technique called potential step. This time, no CO_2 or N_2 was used in the solution (artificial oil field formation water). The investigation using this technique is in agreement with the linear polarization experiments where the 904L and AL-6XN PLUS™ austenitic stainless steels had excellent pitting corrosion resistance when compared with the other austenitic steels (316L and 317L). Figure 8 shows the results of potential step for the 316L, 317L, 904L, and AL-6XN PLUS™ alloys, respectively. The graphs are of type double Y-axis, where the potential (V vs. Ag/AgCl, sat KCl) and the current density (mA/cm^2) are plotted on the Y-axis, and the time (s) is plotted on the X-axis. Every potential step was maintained for one hour. If nothing happened on the passive film, then a new step was reached by an increment of +50 mV. The pitting potential (E_p) of each alloy was achieved when the current density reached values above 0.1 mA/cm^2, as shown on the graphs. So there was an abrupt increase in the current density indicating the breakdown of the passive film. The time to achieve the pitting potential depends on the film resistance of each alloy. The more resistant the passive film, the more time is needed to reach the pitting potential. The pitting potential for the 316L steel presented the lowest value (+0.52 V), while the pitting potential for the 904L and AL-6XN PLUS™ steels presented the highest value (+1.06 V and +1.09 V, respectively). The pitting potential for the 317L steel showed an intermediate value (+0.81 V). Table 3 shows the pitting potential and the time to achieve it for each alloy. It was necessary more than one day for the sample of the AL-6XN PLUS™ steel to reach its pitting potential. This result shows how resistant this material is to the conditions used. On the other hand, the 316L steel presented the lowest time to reach its pitting potential. Even without the presence of CO_2, this steel showed susceptibility to pitting corrosion in chloride-containing environments. The 317L steel showed to be more resistant than the 316L steel in chloride-containing environments but less resistant than the other two super austenitic steels. If compared with table 2, it can be seen that the pH of the solution shifted the pitting potential of the steels. In the presence of CO_2, the solution is more aggressive, decreasing the pitting potential of the steels.

Table 3: Measured pitting potential of the studied alloys using the Potential step technique

Potential step		
Alloy	E(pit) (V Ag/AgCl)	time (h)
316L	+0.52	13.5
317L	+0.81	16.2
904L	+1.06	23.1
AL-6XN PLUS™	+1.09	26.2

The 316L and 317L steels suffered pitting corrosion. For the 316L steel (Figure 9a), the pits possess a circular shape with a center hole. The pit propagates from the center to the edge and tries to grow with time. This effect is attributed to the chloride in the solution. The chloride ion (Cl^-) is very small and can penetrate easily in sites of the 316L surface where the film is broken. The pits on the 316L steel grow but only in the center, as shown in Figure 9a. With the absence

of CO_2 in the solution, the environment is not so aggressive to permit the pits' growth. The 317L steel also suffered pitting corrosion, but its pits are so small compared with the ones of the 316L steel. The pits initiated, but they did not grow with time, as shown in Figure 9b. These pits are non-uniform. This result indicated that the 317L steel in some chloride-containing environments is also resistant, being also a good choice in some applications where the 316L cannot be used, for example, in the oil and gas industry in chloride-containing environments. The super austenitic stainless steels (904L and AL-6XN PLUS™) presented pits much smaller than the ones found on the surface of conventional austenitic steels, as seen in Figure 9 (c-d). They are micro-pits, and after initiating, they passivate again before starting to grow. The effect of CO_2 on the morphology of the pits for the 316L steel, the most affected steel in the experiments, is shown in Figure 10. In Figure 10a, one can see the pits for the potentiodynamic test using CO_2 in the solution. In Figure 10b, it can be seen a single pit formed for the potentiostatic test with no CO_2 in the solution. For the potentiostatic test (potential step), the pit did not grow as expected, leaving a hole in the center. All the micrographs of the alloys taken after the corrosion tests are in accordance by the graphs shown before. This experimental procedure has previously been used to qualify Ni-based alloys and hyper duplex stainless steel for raw seawater injection [14] and also used to study a 13% Cr supermartensitic stainless steel related to localized corrosion [15]. These results combined with the linear polarization tests in CO_2-saturated aqueous solution, show that these materials (the super austenitic stainless steels) are an excellent option for chloride-containing environments with and without CO_2 once they are cheaper than the Ni-based alloys. In some cases, the conventional 317L steel can also be a good option than the conventional 316L steel.

III. Conclusions

It can be concluded that the oil field formation water plays an important role as an aggressive substance in the pre-salt region. In chloride-containing environments, the 316L steel is not so resistant, and it is not recommended for the content of NaCl in the pre-salt region. The type of corrosion found was identified as pitting corrosion. For the 316L steel, pits were formed for both techniques used, but the pitting corrosion was more aggressive for the potentiodynamic technique due to CO_2 in the solution and the absence of free oxygen. The 317L steel presented good pitting corrosion resistance when compared to the 316L steel. The two super austenitic stainless steels studied in this research (904L and AL-6XNPLUS™) presented good pitting corrosion resistance. Both can be the solution for applications in chloride-containing environments as those found in the pre-salt region.

Acknowledgments

The authors would like to thank to the Coordination for the Improvement of Higher Education Personnel (CAPES) and Cearense Foundation to Support Scientific and Technological Development (FUNCAP) for the financial support. A special thank is given to Wilman Italiano, who gave training in the electrochemical tests of potential step and also gave important contributions to this work.

References Références Referencias

1. Race to the sea: the technological and environmental challenges of the pre-salt. Available in:<http://www.coppe.ufrj.br/sites/default/files/coppe_pre-sal.pdf>. (original in Portuguese - access: September 2020).
2. Anselmo N, May JE, Mariano NA, Nascente PAP, Kuri SE. Corrosion behavior of supermartensitic stainless steel in aerated and CO2-saturated synthetic seawater. Mater Sci Eng A 2006;428:73–9.
3. Smith L, Celant M. Martensitic stainless steels in context. Supermartensitic Stainl Steels 2002;2002: 14–20.
4. Cardoso JL, Mandel M, Krüger L, Herculano LFG, Lima Neto P de, Silva MJG da. Corrosion behavior of austenitic stainless steels in CO2-saturated synthetic oil field formation water. Mater Res 2019;22.
5. Cao G, Firouzdor V, Sridharan K, Anderson M, Allen TR. Corrosion of austenitic alloys in high temperature supercritical carbon dioxide. Corros Sci 2012;60:246–55.
6. Firouzdor V, Sridharan K, Cao G, Anderson M, Allen TR. Corrosion of a stainless steel and nickel-based alloys in high temperature supercritical carbon dioxide environment. Corros Sci 2013;69:281–91.
7. Furukawa T, Inagaki Y, Aritomi M. Corrosion behavior of FBR structural materials in high temperature supercritical carbon dioxide. J Power Energy Syst 2010;4:252–61.
8. Russick EM, Poulter GA, Adkins CLJ, Sorensen NR. Corrosive effects of supercritical carbon dioxide and cosolvents on metals. J Supercrit Fluids 1996;9:43–50.
9. Chilingar G V, Mourhatch R, Al-Qahtani GD. The fundamentals of corrosion and scaling for petroleum and environmental engineers. Elsevier; 2013.
10. Eidhagen. J Ku. Eurocorr conference. Crevice Corros. Prop. Sandvik SAF 3207TM HD Dur. Inject. Nat. chlorinated seawater, Stockholm: 2011.
11. Tait WS. An introduction to electrochemical corrosion testing for practicing engineers and scientists. PairODocs Publications; 1994.
12. Bandy R, Cahoon JR. Effect of composition on the electrochemical behavior of austenitic stainless steel in Ringer's solution. Corrosion 1977;33:204–8.

13. Sedriks AJ. Corrosion of Stainless Steels. 2nd ed. New York: John Wiley & Sons; 1996.
14. Eidhagen J, Kivisäkk U. Crevice corrosion properties for Sandvik SAF 3207TM HD during injection of natural and chlorinated seawater, EuroCorr; 2011.
15. Lima LIL, Lima MM, Ferreira M, Nolasco R, de Souza MMD, de Oliveira IA, et al. Preliminary Evaluation of Localized Corrosion Using Potentiodynamic and Potentiostatic Techniques n.d. http://sites.poli.usp.br/org/emcr2012/CD/PDF/Poster/Th-11_Lima.pdf (access: December 2020).

List of Figures

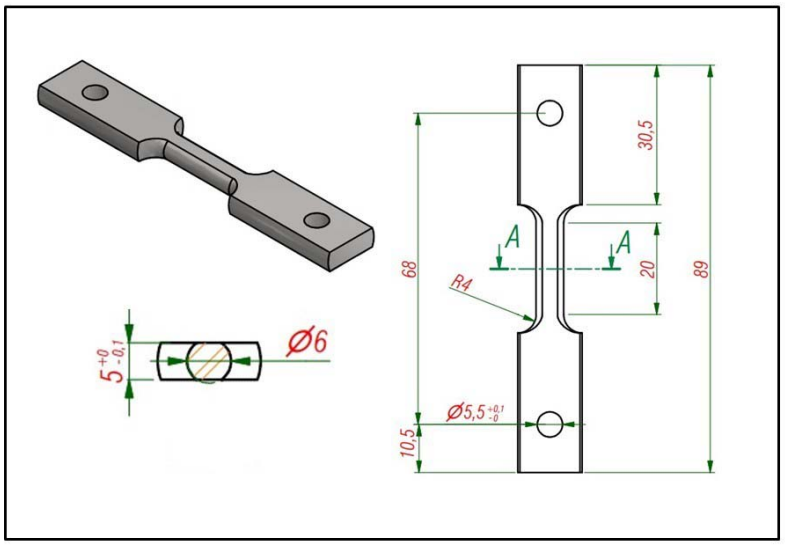

Figure 1: Shape and dimensions (mm) of the samples for the XRD measurements by synchrotron light

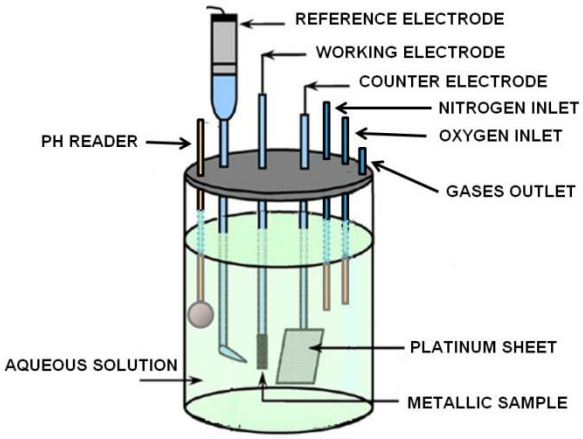

Figure 2: Cell for the CO_2 corrosion test showing all the electrodes used

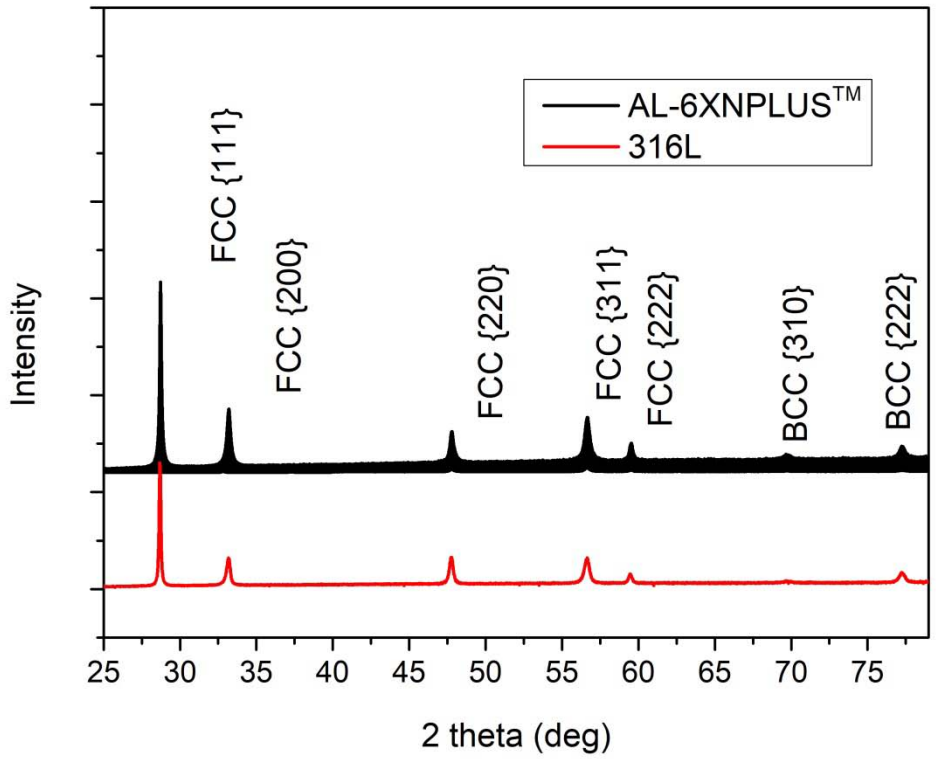

Figure 3: XRD pattern for the 316L and AL-6XNPLUS™ steels in the as-received condition (synchrotron light radiation source, λ = 0.10332 nm)

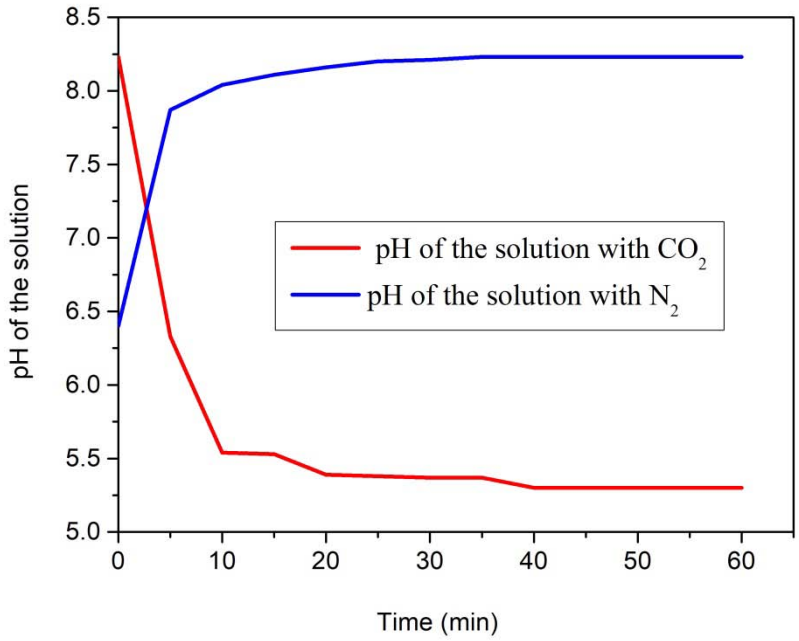

Figure 4: pH of the solution as a function of the bubbling time with N_2 and CO_2

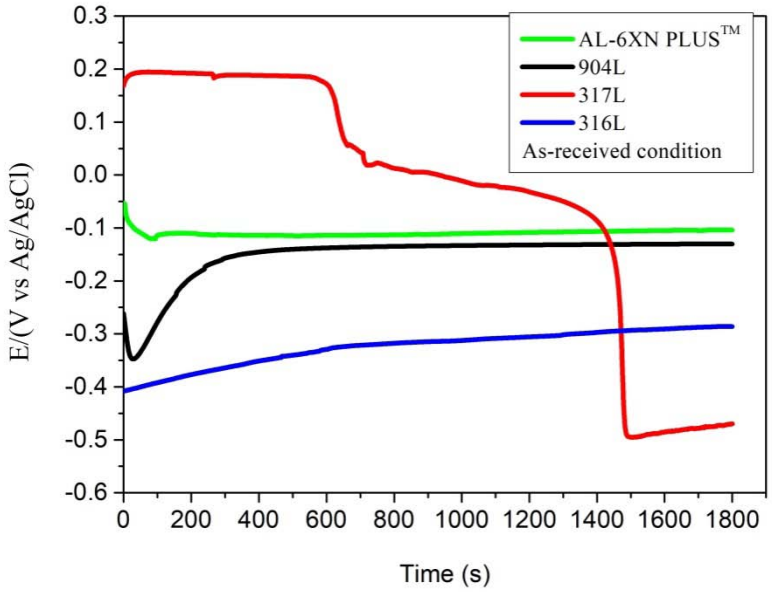

Figure 5: Open circuit potentials for the studied steels

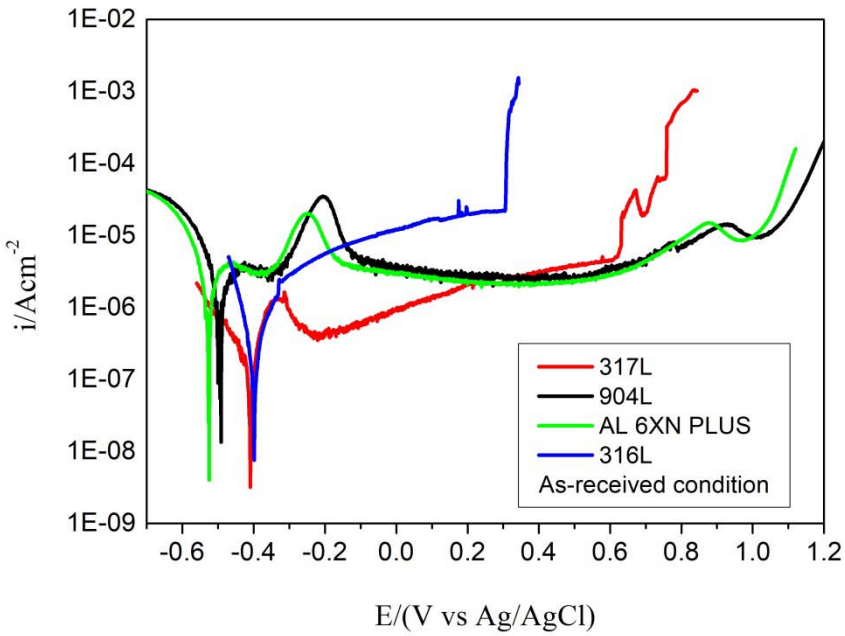

Figure 6: Linear polarization curves for the steels in the as-received condition

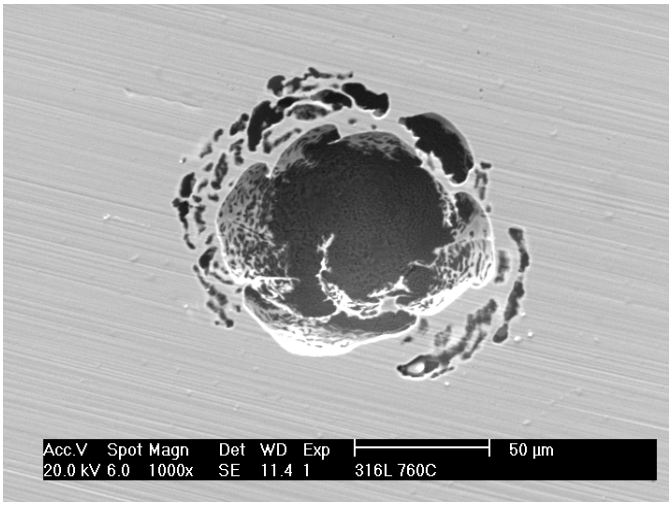

Figure 7: Pit on the surface of the 316L steel after linear polarization tests

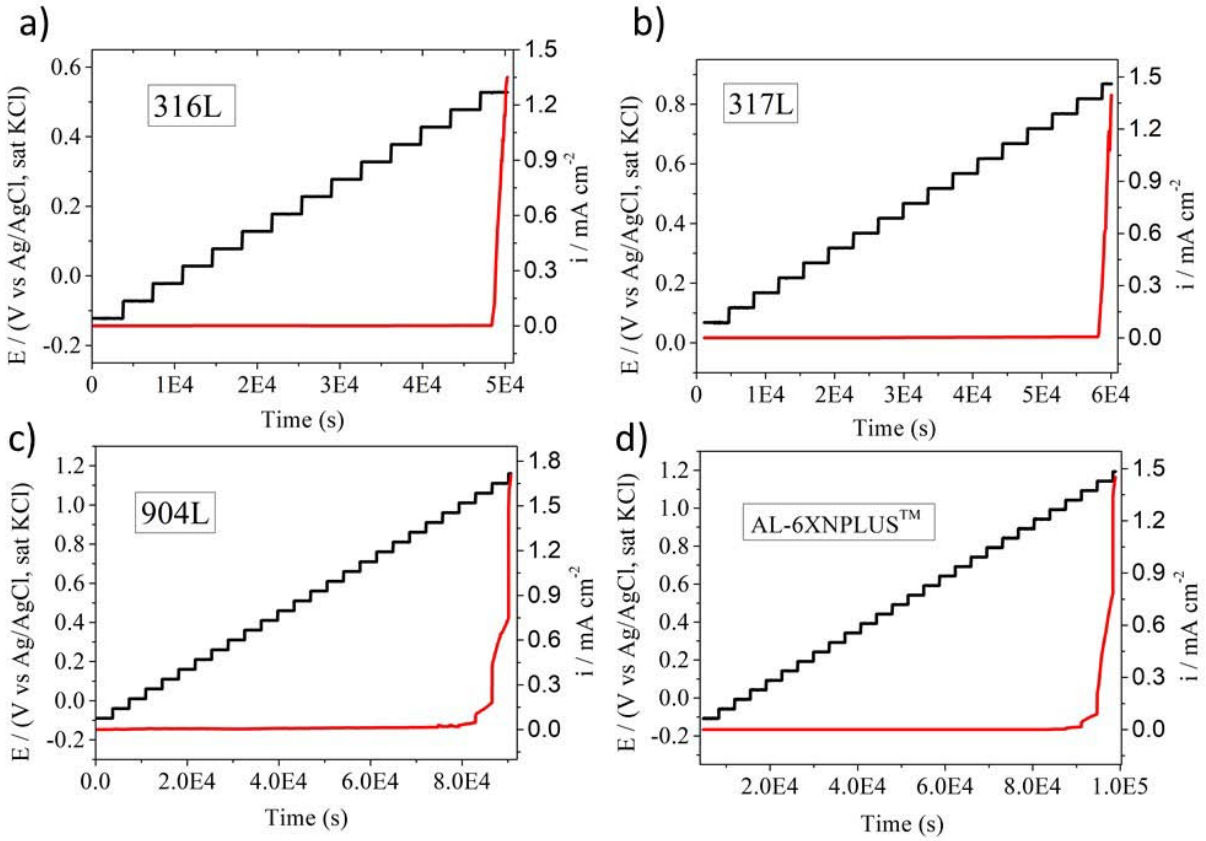

Figure 8: Plots with the potential steps, current density and time for the studied alloys in artificial oil field formation water

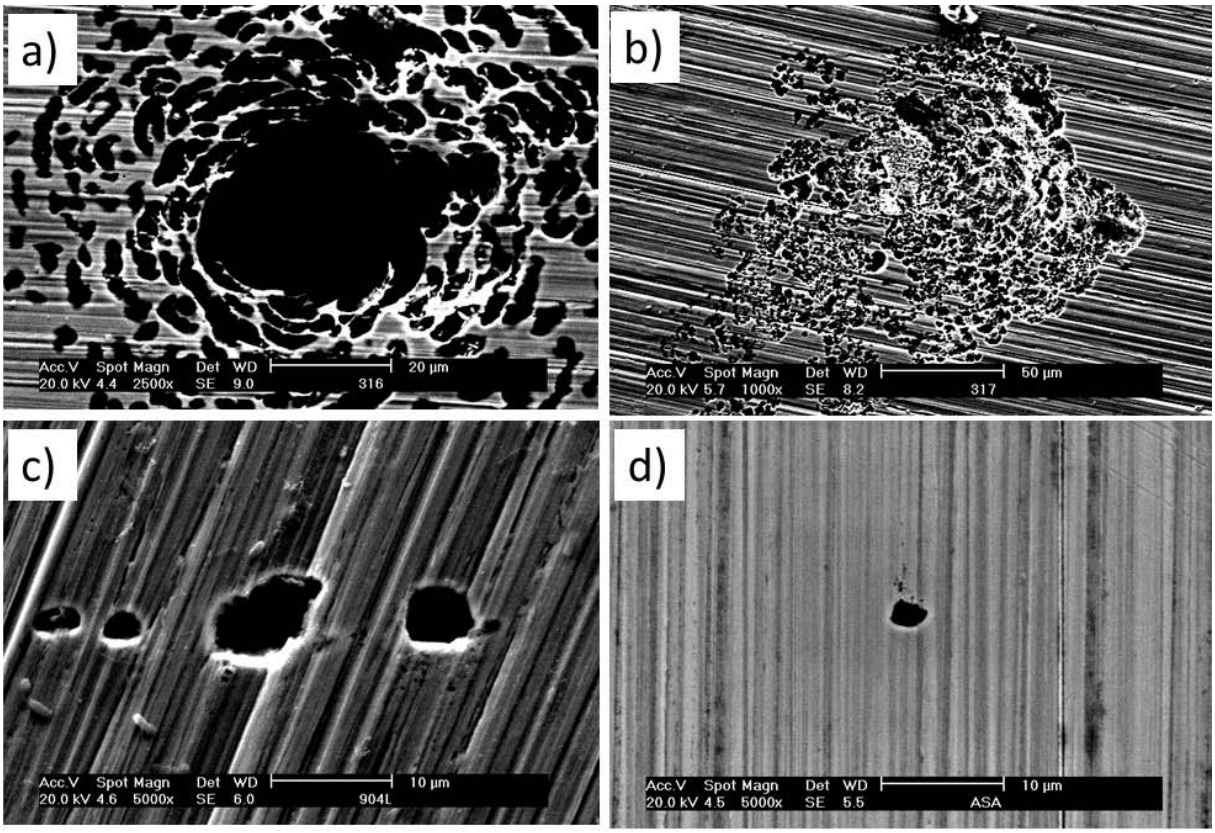

Figure 9: SEM image showing the pits formation on the surfaces of the studied alloys, a) 316L, b) 317L, c) 904L and d) AL-6XNPLUS™